THE JOURNAL OF BIOLOGICAL CHEMISTRY VOL. 289, NO. 46, pp. 31765–31776, November 14, 2014

Biochemical and Biophysical Characterization of the Selenium-binding and Reducing Site in *Arabidopsis thaliana* Homologue to Mammals Selenium-binding Protein 1*[S]

Received for publication, April 16, 2014, and in revised form, September 17, 2014 Published, JBC Papers in Press, October 1, 2014, DOI 10.1074/jbc.M114.571208

Florie Schild[‡], Sylvie Kieffer-Jaquinod[§], Andrés Palencia[¶], David Cobessi[‖1], Géraldine Sarret[1], Chloé Zubieta[‡1], Agnès Jourdain[‡1], Renaud Dumas[‡1], Vincent Forge[‡‡], Denis Testemale[§§], Jacques Bourguignon[‡], and Véronique Hugouvieux[‡2]**

From the [‡]Institut de Recherches en Technologies et Sciences pour le Vivant, Laboratoire de Physiologie Cellulaire et Végétale, CEA, Université Grenoble Alpes, CNRS UMR5168, INRA USC1359, the [§]Institut de Recherches en Technologies et Sciences pour le Vivant, Laboratoire de Biologie à Grande Echelle, Université Grenoble Alpes, CEA, INSERM, 17 rue des Martyrs, F-38000 Grenoble, France, the [¶]European Molecular Biology Laboratory Outstation, 71 avenue des Martyrs, F-38042 Grenoble, France and Unit for Virus Host-Cell Interactions, Université Grenoble Alpes-EMBL-CNRS, 71 avenue des Martyrs, 38042 France, the [‖]Université Grenoble Alpes, CEA, CNRS, Direction des Sciences du Vivant, Institut de Biologie Structurale, 6 rue Jules Horowitz, F-38044 Grenoble, France, the [**]Université Grenoble Alpes, CNRS & IRD, ISTerre, BP 53, F-38041 Grenoble, France, the [‡‡]Laboratoire de Chimie et Biologie des Métaux, Université Grenoble Alpes, CEA, CNRS, Institut de Recherches en Technologies et Sciences pour le Vivant, 17 rue des Martyrs, F-38000 Grenoble, France, and the [§§]Université Grenoble Alpes, CNRS, Institut NEEL, 25 rue des Martyrs, F-38042 Grenoble, France

Background: The selenium-binding site in selenium-binding protein (SBP) homologues was not identified.
Results: The *Arabidopsis thaliana* SBP1 selenium-binding site was characterized as a R-S-Se(II)-S-R-type complex involving Cys^{21} and Cys^{22}.
Conclusion: This is the first identification of the selenium-binding site in any SBP.
Significance: It is an important step toward a better understanding of the link between selenium binding and function of SBP.

The function of selenium-binding protein 1 (SBP1), present in almost all organisms, has not yet been established. In mammals, SBP1 is known to bind the essential element selenium but the binding site has not been identified. In addition, the SBP family has numerous potential metal-binding sites that may play a role in detoxification pathways in plants. In *Arabidopsis thaliana*, *At*SBP1 over-expression increases tolerance to two toxic compounds for plants, selenium and cadmium, often found as soil pollutants. For a better understanding of *AtSBP1* function in detoxification mechanisms, we investigated the chelating properties of the protein toward different ligands with a focus on selenium using biochemical and biophysical techniques. Thermal shift assays together with inductively coupled plasma mass spectrometry revealed that *At*SBP1 binds selenium after incubation with selenite (SeO_3^{2-}) with a ligand to protein molar ratio of 1:1. Isothermal titration calorimetry confirmed the 1:1 stoichiometry and revealed an unexpectedly large value of binding enthalpy suggesting a covalent bond between selenium and *At*SBP1. Titration of reduced Cys residues and comparative mass spectrometry on *At*SBP1 and the purified selenium-*At*SBP1 complex identified Cys^{21} and Cys^{22} as being responsible for the binding of one selenium. These results were validated by site-directed mutagenesis. Selenium K-edge x-ray absorption near edge spectroscopy performed on the selenium-*At*SBP1 complex demonstrated that *At*SBP1 reduced SeO_3^{2-} to form a R-S-Se(II)-S-R-type complex. The capacity of *At*SBP1 to bind different metals and selenium is discussed with respect to the potential function of *At*SBP1 in detoxification mechanisms and selenium metabolism.

At low concentration, selenium is an essential nutrient to many organisms including some archaea, bacteria, protozoan, green algae, and nearly all animals but it is non-essential in land plants (1–4). The daily selenium requirement in human adults is 60 to 70 μg and the main source of dietary selenium is plants (3, 5). Selenium dietary consumption has been associated with a reduced risk of many diseases such as cardiovascular diseases, diabetes, and cancer. In addition, a lack of selenium can lead to Keshin-Beck and Keshan disease that can be treated by selenium supplementation (3, 4). In organisms where selenium is an essential nutrient, it is required for the biosynthesis of the selenoamino acid selenium-Cys, used for the translation of 25 selenoproteins, which are involved in critical functions such as redox reactions, free radical scavenging, and hormone regulation (1, 3, 4). In addition to its role as a micronutrient, selenium can have toxic effects. Selenium toxicity (selenosis) can occur in some areas where exploitation of seleniferous soils or fossil fuels leads to toxic accumulation of selenium in the environment and in plants. In mammals, excess selenium targets the cardiovascular, gastrointestinal, neurological, and hematopoietic systems (3, 5–7). As the line between selenium deficiency

* This work was supported by the Rhône-Alpes region, the Biologie et Amélioration des Plantes Department of Institut National de la Recherche Agronomique, and the CEA Toxicology program.
[S] This article contains supplemental Table S1.
[1] These authors contributed equally to this work.
[2] To whom correspondence should be addressed. Tel.: 33-4-38-78-06-54; Fax: 33-4-38-78–5091; E-mail: Veronique.hugouvieux@cea.fr.

and toxicity is very narrow, both selenium deficiency and selenium toxicity are common problems worldwide.

Selenium concentration in soils ranges from 0.01 to 2 mg/kg and can be >10 mg/kg in seleniferous soils (3, 5, 8). When present in soil, selenium is absorbed and accumulated in plants and is subsequently disseminated along the whole food chain. In this context, plants may help to alleviate both selenium deficiency and toxicity problems. A better understanding of the mechanisms involved in the plant response to selenium including accumulation, protection, and sequestration can be considered as one of the most important challenges in the coming decades. Engineering plants with nutrient-enriched content for biofortification, using plants to remove toxic selenium for phytoremediation and selecting for selenium resistant plants are critical goals (5, 8).

The impact of selenium on plant physiology has been extensively studied. Selenium is not essential to land plants, unlike in mammals. Plant homologues to selenoproteins from mammals and bacteria have a Cys residue in their sequence instead of selenocysteine. However, low concentrations of selenium can have a positive effect on plant growth and be beneficial in facing biotic and abiotic stress (9, 10) notably by protecting plants against oxidative stress. At higher concentrations, selenium is generally highly toxic to plants.

The major forms of inorganic selenium in soils are Se(VI) (SeO_4^{2-}) and Se(IV) (SeO_3^{2-}), which are taken up by roots via sulfate and phosphate transporters, respectively (6, 11). Once inside the cells, selenium toxicity results from its chemical similarity with sulfur that leads to nonspecific replacement of sulfur containing amino acids with their seleno derivatives (7, 12, 13). In addition, at high concentrations, selenium triggers oxidative stress by reducing the pool of glutathione (GSH) (12). The main mechanisms of selenium tolerance in plants are the conversion of SeMet and SeCys into their methylated forms, which are non-incorporable into proteins, and volatilization (5, 8).

In addition to its incorporation into selenoproteins, selenium can be bound to proteins belonging to the selenium-binding protein family (SBP).[3] Many of the beneficial impacts of selenium on mammalian health have been attributed to its role as a critical constituent of selenoproteins and to its binding to SBP1. Although the function of selenoproteins is well established, the activity of SBP1 proteins is still unclear and the link between selenium binding and SBP1 function has not yet been determined. Mammalian SBP1 was first identified in mouse liver (14) in experiments designed to find new selenoproteins. Two homologues are present in humans. Today, *SBP* genes have been identified in many organisms including plants (14–18) and additional sequences of SBP homologues are available in public databases from many additional organisms. In humans, down-regulation of *SBP1* expression has been correlated with rapid tumor development in many organs (19–27) and *SBP1* expression is considered to be a predictor of clinical outcome. Recently, interaction of SBP1 and the selenoprotein glutathione peroxidase GPx-1 was observed, revealing a cross-talk between members of distinct families of selenium containing proteins (19, 21, 28). SBP1 was also characterized as a biomarker for schizophrenia as up-regulation of *SBP1* is observed in the brains of patients with the disease (29, 30). Other functions, such as intra-Golgi protein transport have been assigned to mammalian SBP1 (31). Its SBP2 homologue was described as playing a protective role as a scavenger of toxic electrophiles or oxidant species (32–34).

In the *Arabidopsis thaliana* genome, 3 genes encoding SBP are present (16). *At*SBP1 is the isoform that is the most highly expressed (35). One of the first functions that was assigned to SBP1 in plants was a putative role in selenium tolerance (15). Indeed, plants over-expressing *AtSBP1* have increased resistance to selenite (SeO_3^{2-}), whereas reducing *At*SBP1 and *At*SBP2 expression increased plant sensitivity to the toxic compound (15). *At*SBP1 could therefore be involved in selenium metabolism but no reports were available in the literature on the ability of *At*SBP1 to bind selenium like its mammalian homologues.

In addition to its putative role in selenium tolerance, *At*SBP1 has been identified as a protein accumulating in response to the heavy metal cadmium in *A. thaliana* cultured cells using differential proteomic analysis (36). Cadmium is toxic to most organisms and is one of the most toxic pollutants in the world. One of the main mechanisms that plants use to face cadmium toxicity is the synthesis of polymers of GSH, called phytochelatines, that chelate cadmium and are then transferred into the vacuoles (37). *At*SBP1 shows the ability to bind 3 cadmium *in vitro* and *At*SBP1 over-expression in *A. thaliana* seedlings led to enhanced tolerance to cadmium (35). This phenotype is more important in GSH- and phytochelatine-deficient *Arabidopsis* seedlings (35). Therefore, *At*SBP1 may have chelating properties *in vivo* toward cadmium and may represent a new detoxification mechanism that plants use to face heavy metal toxicity, possibly throught direct binding to the metal (35). In addition to cadmium, *AtSBP1* over-expressing *A. thaliana* plants showed increased tolerance to stress such as selenium and H_2O_2 that also require GSH for detoxification (38). Overexpression of *Os*SBP1 in rice enhanced tolerance to various pathogens (17) and the importance of GSH in plant defense to biotic stress has been recently reviewed (39). These results suggest that SBP1 may share similar functions with GSH in response to stress. In line with these results, stresses inducing *SBP1* expression were also inducers of *PRH43*, which encodes 5′-adenylylphosphosulfate reductase 2, a key enzyme of the sulfur assimilation pathway and GSH biosynthesis (38). As an example, *AtSBP1* and *AtPRH43* are induced by cadmium, SeO_4^{2-}, H_2O_2 and sulfur starvation. An internal sulfur demand of the cell could be a signal that triggers SBP1 expression in response to the different stresses (37) and this correlates well with the potential functional redundancy between SBP1 and GSH.

To date, all the data accumulated on SBP1 function in plants points to the importance of SBP1 in response to stress. The fact that *At*SBP1 shows the ability to bind cadmium, a toxic metal,

[3] The abbreviations used are: SBP, selenium-binding protein; TSA, thermal shift assay; ICP-MS, inductively coupled plasma mass spectrometry; XANES, K–edge X ray absorption near edge structure spectroscopy; DTNB, 5,5′-dithiobis-(2-nitrobenzoic acid); GSH, Glutathione; ITC, isothermal titration calorimetry.

in vitro, and that the mammalian homologue can bind selenium *in vivo*, another toxic compound for plants, raises the question of whether *At*SBP1 may have some chelating properties toward selenium as well as other metals in addition to cadmium. Because of the importance of selenium in human health, and the critical function of SBP1 in selenium tolerance in plants, we focused on the identification of the selenium-binding site in *At*SBP1. By using complementary biochemical, spectroscopic, and biophysical approaches, we characterized the selenium and metal binding properties of *At*SBP1. These data identify, for the first time, the selenium-binding site in any SBP1 homologues. Its characterization provides evidence that two Cys residues are involved in selenium binding and that *At*SBP1 reduces selenite (SeO_3^{2-}). This work provides an important step toward a better understanding of SBP1 function in selenium metabolism, detoxification, and accumulation mechanisms in plants.

EXPERIMENTAL PROCEDURES

*Overexpression of AtSBP1 in Escherichia coli and Purification of the Recombinant Protein—At*SBP1 cDNA contained in the entry clone (U15803, TAIR database) was cloned into the destination pGEX-3X for GST-*At*SBP1 production as previously described (35). The recombinant plasmid was used to transform *E. coli* strain Rosetta 2. Cell cultures were grown at 37 °C in Luria-Bertani medium until an $A_{600\ nm}$ of 0.8. The temperature was then lowered to 18 °C and expression of the recombinant protein was induced by adding 0.8 mM isopropyl β-D-thiogalactopyranoside to the cultured cells for 17 h. Cells were then centrifuged and stored at −80 °C. For protein purification, cells were lysed by sonication (6 × 1 min, using the Branson Sonifier 250) in 20 mM HEPES, pH 7.4, 150 mM NaCl, 0.05% Triton X-100 (v/v), 10% glycerol (v/v), and 1 mM DTT. The recombinant GST-SBP1 protein was purified via affinity chromatography using GSH-Sepharose 4B resin according to the manufacturer's instructions (GE Healthcare). The GST tag was removed by incubating GST-*At*SBP1 with Factor Xa (Sigma) for 15 h at 22 °C in 50 mM Tris, pH 8.0, 150 mM NaCl, and 1 mM $CaCl_2$. Factor Xa was depleted by binding to *p*-aminobenzamidine-agarose (Sigma). *At*SBP1 was further purified using size exclusion chromatography on an AKTA purifier system (Amersham Biosciences) and an S200 16/60 column (HiLoad 16/60, Superdex 200, Amersham Biosciences). Unless otherwise stated, all the experiments were performed using cleaved *At*SBP1.

Site-directed Mutagenesis—Site-directed mutagenesis were produced from the template GST-*At*SBP1 contained in the PGEX-3X vector. Primer sequences were designed using QuikChange Primer Design software from Agilent Technology. Cys^{21} and Cys^{22} of *At*SBP1 were replaced by Ser residues. PCR was performed using Phusion enzyme with 18 cycles as follow: 30 s at 98 °C, 1 min at 55 °C, and 1 min 40 s at 72 °C. PCR products were incubated 1 h at 37 °C with DpnI and used to transform *E. coli* strain DH5α. Plasmids were extracted with Nucleospin Plasmid kit and sequenced by Eurofins (Les Ulis, France).

Stability Analysis of Recombinant AtSBP1 by Thermal Shift Assay (TSA)—Temperature stability analysis was conducted with recombinant *At*SBP1 protein using 96-well plates. *At*SBP1 (5 μM) was incubated with Sypro Orange (diluted 1/1000 from S6650 solution; Invitrogen) as described (40) and 2 concentrations of Cd^{2+}, SeO_3^{2-}, Zn^{2+}, Ni^{2+}, Co^{2+}, Cu^{2+}, SeO_4^{2-}, Mn^{2+}, Mg^{2+}, and MoO_4^{2-} ranging from 1 to 25 μM (prepared from $Cd(NO_3)_2$, Na_2SeO_3, $ZnCl_2$, $NiCl_2$, $Co(NO_3)_2$, $CuCl_2$, Na_2SeO_4, $MnCl_2$, $MgCl_2$, and Na_2MoO_4, respectively) in 50 mM HEPES, 150 mM NaCl, pH 7.4, overnight at 4 °C. Experiments were performed in a final volume of 25 μl. Samples were heated from 25 to 75 °C with a rate of 1 °C per min using the thermocycler Stratagene Mx3005P. Excitation and emission wavelengths were 492 and 516 nm, respectively. The melting temperature corresponded to the temperature indicated at half of the Δfluorescence (final fluorescence − initial fluorescence).

Metal and Selenium Binding Assay by Inductively Couple Mass Spectrometry (ICP-MS)—To determine the metal or selenium to protein molar ratio, 2 nmol of recombinant *At*SBP1 protein were incubated for 15 min at 25 °C with 25 nmol of Cd^{2+}, Zn^{2+}, Ni^{2+}, or SeO_3^{2-} in a total volume of 25 μl containing 10 mM HEPES, pH 7.4, and 150 mM NaCl. *At*SBP1-bound species were separated from free ions by steric exclusion chromatography through a Sephadex G-25 column (0.5 × 8.5 mm) with an elution rate of 150 μl/min. Fractions of 200 μl were collected. Protein elution was followed using a spectrophotometer (NanoDrop 2000, Thermoscientific) at 280 nm, and metal and selenium content was assayed by inductively coupled plasma-mass spectrometry (ICP-MS; HP4500 Chemstation; Yokogawa Analytical System). Isotopes 64, 66, 77 and 82, and 112 were monitored for zinc, nickel, selenium, and cadmium quantification, respectively. ICP-MS experiments were performed in 0.1% HNO_3 (v/v).

Isothermal Titration Calorimetry (ITC) Experiments and Determination of Thermodynamic Parameters—Determination of Se-*At*SBP1 thermodynamic parameters was carried out by calorimetric experiments with recombinant GST-*At*SBP1 and GST alone. SeO_3^{2-} (0.5 and 2 mM) was added by successive injections (1.5 μl) to GST-*At*SBP1 (50 μM) in a total volume of 0.22 ml. Buffer conditions were 10 mM HEPES, pH 7.4, and 150 mM NaCl. Calorimetric titrations were performed at 25 °C with stirring at 800 rpm using a microcalorimeter (Microcal ITC 200 System, GE Healthcare). Data were analyzed with Origin ITC 200 software. Independent duplicates were performed with GST-*At*SBP1. ITC experiments with GST alone were run in parallel to confirm that GST alone did not bind SeO_3^{2-}. A further experiment was conducted with cleaved *At*SBP1 that confirmed results obtained with GST-*At*SBP1.

Cysteine Quantification Using DTNB—For reduced cysteine titration, *At*SBP1 (8 μM) was incubated for 30 min at room temperature in the dark with 5,5′-dithiobis-(2-nitrobenzoic acid) (DTNB) (1.6 mM) in a total volume of 60 μl containing 10 mM HEPES, pH 7.4, and 150 mM NaCl. Cysteine quantification was determined by measuring the absorbance at 412 nm using a spectrophotometer (NanaDrop 2000, Thermo Scientific). For buried cysteine quantification, *At*SBP1 was unfolded in urea (8 M). For cysteine quantification after selenium binding, *At*SBP1 was incubated with the SeO_3^{2-} (100 μM) for 15 min at 25 °C prior to DTNB treatment.

*Secondary Structure Modifications after Incubation of AtSBP1 with SeO_3^{2-} using Circular Dichroism (CD)—At*SBP1 (2.7 μM) was incubated with or without SeO_3^{2-} (33.5 μm) in a

total volume of 1.5 ml containing 10 mM HEPES, pH 7.4, and 150 mM NaCl. Spectra acquisition was performed at 25 °C using a spectropolarimeter (J-815, Jasco) in the far UV (200–260 nm) with the following parameters: 1 nm step, 2 nm bandwidth, and scan speed 200 nm/min. The optical path length was 1 mm.

Model Building—The three-dimensional model was generated using Chimera and Modeler version 9.10. The sequence of At4g14030 was aligned with sequences from the Protein Data Bank using Blast and Blosum62 as the alignment matrix. The structure of the hypothetical selenium-binding protein from *Sulfolobus tokodaii* (PDB entry 2ECE) was the closest homologue and used to generate a three-dimensional model with the program Modeler (*E*-value of 7e-86; 40% sequence identity). The model of At4g14030 with the lowest discrete optimized protein energy score was selected.

Infusion MS Analysis of AtSBP1 and Selenium-AtSBP1 Complex—After incubation of *At*SBP1 with SeO_3^{2-}, fractions containing selenium-bound *At*SBP1 and native *At*SBP1 were purified by pure water exchange using the Vivaspin 500 (Sartorius) system and analyzed by nano-electrospray in direct injection at a concentration of 1 μM. MS analysis was performed within the Linear Trap Quadrupole of a LTQ-Orbitrap-XL. The theoretical average mass was calculated using the Isotope simulation from Xcalibur 2.2 (Thermo Scientific) in the profile mode and using a resolving power of 1000. Multicharged spectra were externally recalibrated and deconvoluted using the Hyper Mass transform algorithm implemented in ICR-2LS (PNNL, Richland, WA).

Nano-LC-MS/MS Analysis of Chymotrypsic Peptides of AtSBP1 and Selenium-AtSBP1 Complex—After incubation of GST-*At*SBP1 with SeO_3^{2-}, fractions containing selenium-bound GST-*At*SBP1 or GST-*At*SBP1 alone were digested with diluted chymotrypsin in 25 mM ammonium bicarbonate (100 ng for 2 μg of GST-SBP1) for 15 h at 37 °C. Digested peptides were dried under vacuum on a centrifugal evaporator. One hundred ng of the dried extracted peptides were solubilized in water containing 5% acetonitrile and 0.1% formic acid before being transferred to a glass vial for a nano-LC-MS/MS analysis (Ultimate 3000, Dionex and LTQ Orbitrap Velos Pro, ThermoFisher Scientific). The LC method consisted of a 30-min separation at a flow rate of 300 nl/min using a binary solvent gradient: A (2% acetonitrile and 0.1% formic acid in water) and B (80% acetonitrile and 0.1% formic acid in water). The system included a 300 μm × 5-cm PepMap C18 precolumn for preconcentration and desalting of the peptides and a 75 μm × 15-cm PepMap C18 column (Dionex) for peptide separation and elution. MS and MS/MS data were acquired using XCalibur software (ThermoFisher Scientific) in the positive ion electrospray ionization mode with a resolution of 60,000 full-width half-maximum in the MS mode. Peak list generation was first performed using MASCOT Distiller and consecutive searches against a database containing the GST-SBP1 sequence were performed using MASCOT 2.4. The parameters used with MS/MS transformed data (.mgf) were: instrument = ESI-TRAP; enzyme = no; oxidation (M); selenium (CDHM); deamination (NQ); disulfide (C); peptide tolerance = 10 ppm; fragment tolerance = 0.6 Da. Results were filtered using IRMa software (41). Every peptide having a Mascot score below 18 was filtered. The isotope simulation feature of Xcalibur was used to simulate the isotopic profiles of peptides of interest with and without selenium.

X-ray Absorption Spectroscopy on the Selenium-AtSBP1 Complex—X-ray absorption measurements were carried out at the European Synchrotron Radiation Facility (ESRF, Grenoble, France) at a ring current of 150–200 mA. Spectra were collected on the BM30B (FAME) beamline (42) using a Si(220) double crystal monochromator with dynamic sagittal focusing. The photon flux was 10^{11} photons/s and the spot size was 300 μm horizontal × 100 μm vertical (full width half-maximum values). Selenium K-edge x-ray absorption near edge structure (XANES) spectra were recorded for a 1.6 mM solution of purified selenium-*At*SBP1 in 10 mM HEPES, pH 7.4, 150 mM NaCl, and 20% glycerol (v/v), and for various selenium reference compounds including SeO_3^{2-}, SeS_2, selenomethylcysteine (selenium-Met-Cys, R-Se(II)-R), and selenomethionine (selenium-Met, R-Se(II)-R). Spectra for gray Se(0) and selenodiglutathione (selenium-diGSH, R-S-Se(II)-S-R) were recorded previously on the same beamline in the same experimental conditions (43). All solid compounds were diluted in Boron Nitride to reach 5000 μg g^{-1} of selenium, and pressed as pellets. For the selenium-*At*SBP1 sample, 40 μl of the solution was transferred to a five-cell sample holder with a kapton window, and flash frozen in liquid nitrogen. Solid pellets were loaded in the same sample holder, which was then transferred to a helium cryostat with temperature set around 10 K during data collection. For each sample, four to six scans of 20 min were averaged. The position of the beam on the pellet was moved between each scan to limit radiation damage. All spectra were collected in fluorescence mode measuring the selenium Kα fluorescence with a 30-element solid-state Ge detector (Canberra). Energy calibration was achieved by measuring a selenium foil and assigning the first inflection point of the spectrum to 12658 eV for selenium. Data analysis was performed using Athena software. After normalization, the spectrum for the selenium-*At*SBP1SBP1 complex was fitted by linear combination of selenium reference compounds in the 12,640–12,700 eV range.

RESULTS

Analysis of AtSBP1 Thermostability and Chelating Properties Toward Different Metals and Selenium—To determine whether *At*SBP1 was able to bind different ionic species, thermal shift assays were used to screen binding of different ions. As shown in Fig. 1, the T_m of *At*SBP1 is about 45 °C. It reproducibly shifts by about 3 °C in the presence of Cd^{2+} and >3 °C in the presence of Zn^{2+}, Ni^{2+}, Cu^{2+}, and Co^{2+}. A slight but very reproducible enhanced T_m (around 1 °C) was observed in the presence of Mo(VI) (MoO_4^{2-}) at 25 μM and Se(IV) (SeO_3^{2-}) at 5 μM, but not with Se(VI) (SeO_4^{2-}). We verified that the increased T_m was correlated with binding of the ions to *At*SBP1 by determining the ion to protein molar ratio by ICP-MS for SeO_3^{2-}, Cd^{2+}, and two additional selected ionic species (Zn^{2+} and Ni^{2+}) (Fig. 2). As shown in Fig. 2, *At*SBP1 shows the ability to bind one selenium *in vitro* when incubated with SeO_3^{2-}, and three Cd^{2+}, three Ni^{2+} and three Zn^{2+} ions. No binding of selenium was observed when incubated with SeO_4^{2-} (data not shown). Although *At*SBP1 exhibits promiscuous binding to dif-

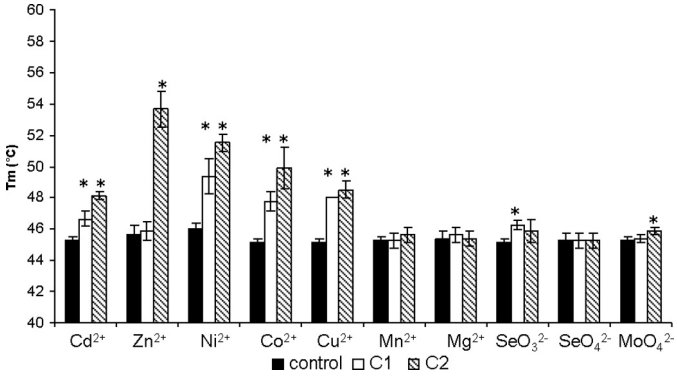

FIGURE 1. **Identification of ions that stabilize *A. thaliana* SBP1.** *At*SBP1 melting temperature was determined by TSA experiments. *At*SBP1 (5 μM) was incubated with Sypro Orange and Cd^{2+}, SeO_3^{2-}, Zn^{2+}, Ni^{2+}, Co^{2+}, SeO_4^{2-}, Mn^{2+}, Mg^{2+}, and MoO_4^{2-} at 5 (*C1*) or 25 μM (*C2*) and Cu^{2+} at 1 (*C1*) and 5 μM (*C2*). Each experiment of TSA was performed in duplicates providing two sets of values per ion concentration. Data show the mean ± S.D. of two independent TSA experiments. *, represents statistical difference compared with control condition with no ion evaluated by Student's *t* test.

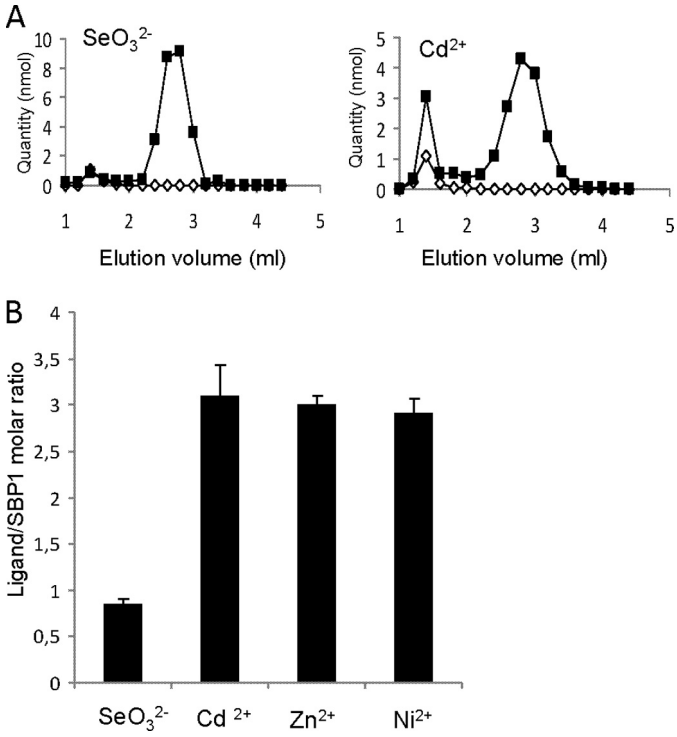

FIGURE 2. ***In vitro* binding capacity of *A. thaliana* SBP1 toward SeO_3^{2-}, Cd^{2+}, Zn^{2+}, and Ni^{2+}.** Two nmol (80 μM) of recombinant *At*SBP1 were incubated with 25 nmol (1 mM) of SeO_3^{2-}, Cd^{2+}, Zn^{2+}, and Ni^{2+} in a final volume of 25 μl. Ligand-bound *At*SBP1 was separated from the free ligand by steric exclusion chromatography on a Sephadex G-25 column. The concentration of the eluted SBP1 was followed by measuring the A_{280} (*white square*), and ligand content was measured by ICP-MS (*black square*). *A*, representative elution profiles are shown for SeO_3^{2-} and Cd^{2+}. *B*, values of the ligand/*At*SBP1 molar ratio evaluated on 3 independent experiments.

ferent metal ions *in vitro*, its ability to bind selenite could be critical for its *in vivo* function, as *At*SBP1 expression level regulates selenium tolerance in *A. thaliana* (15). The chelating properties of *At*SBP1 toward selenium were therefore investigated.

Thermodynamic Parameters of Selenium Interactions with AtSBP1—Isothermal titration calorimetry was used to study the binding of SeO_3^{2-} to *At*SBP1. This technique allows the

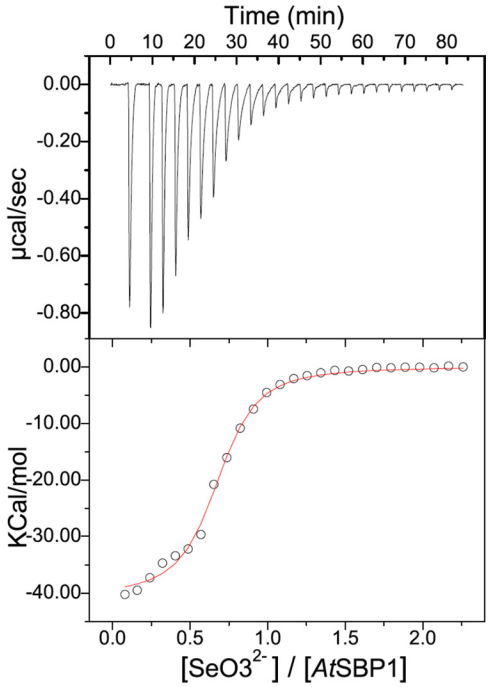

FIGURE 3. **Isothermal titration calorimetry experiments showing the binding of SeO_3^{2-} to *A. thaliana* SBP1.** *Top panel* shows titration of SeO_3^{2-} at 0.5 mM into *At*SBP1 at 50 μM placed at the sample cell. *Bottom panel* shows the ligand concentration dependence of the heat released upon binding after normalization. The data were fitted to one-site binding model.

determination, in one titration, of the stoichiometry, affinity, and enthalpic or entropic contributions to the Gibbs free energy. ITC curves and thermodynamic parameters obtained during the interaction of SeO_3^{2-} and *At*SBP1 are shown in Fig. 3 and Table 1, respectively. For each SeO_3^{2-} injection, a release of heat was observed (Fig. 3, *upper panel*) indicating a clear binding event between SeO_3^{2-} and *At*SBP1. Furthermore, the binding isotherms could be fitted unambiguously to a one-site binding model (Fig. 3, *lower panel*), which allowed us to determinate an apparent binding constant in the low micromolar range (1.6 μM). We also estimated the number of sites as ~0.75, therefore confirming the 1:1 stoichiometry of the interaction determined by ICP-MS. Unexpectedly, the binding enthalpy value measured for SeO_3^{2-} binding was −51,720 cal/mol, which is extremely high only taking into account the limited number of polar interactions that a single ion could establish with *At*SBP1 (see for comparison examples of other ionic species and proteins (44–46)). Therefore, the strong negative enthalpy difference values obtained for SeO_3^{2-} most likely correspond to a combination of a binding event with a specific covalent reaction between the protein and SeO_3^{2-}. This is also supported by the fact that the calorimetric signals needed abnormally large times to recover to the baseline value (broadening of the peaks), suggesting that a covalent reaction was coupled with the binding of the ion.

Impact of Selenium on Cysteine Titration and Secondary Structure of SBP1—Selenium can interact with cysteine (Cys) residues (47, 48). Titration of reduced and accessible Cys residues was performed on *At*SBP1 alone and *At*SBP1 incubated with SeO_3^{2-} using DTNB (Fig. 4*A*). The *At*SBP1 protein sequence contains 7 Cys residues. In the native *At*SBP1 protein,

TABLE 1

Thermodynamic parameters calculated from microcalorimetric experiments for the interaction between SeO_3^{2-} and *A. thaliana* SBP1 at 25 °C in 10 mM HEPES, pH 7.4, 150 mM NaCl

Independant experiments were carried out with 2 and 0.5 mM solutions of SeO_3^{2-} titrated to *At*SBP1 at 50 μM. Thermodynamic parameters represent the average from at least two independent experiments (estimated errors are about 5%) obtained by fitting the data to a one-site binding model. Parameters were calculated with the software Origin ITC 200. *K* represents the apparent binding constant.

	K (M^{-1})	ΔG (cal/mol)	ΔH (cal/mol)	$-T\Delta S$ (cal/mol)
ITC moyen	609,500	−7,753	−51,720	43,955

4 free accessible Cys residues were titrated and 5 in the urea-treated protein indicating that one reduced Cys residue was therefore not accessible and two others would be involved in a disulfide bridge. In the presence of SeO_3^{2-}, only two free accessible Cys residues were detected, indicating that selenium binding was strongly stable and would involve two accessible and reduced Cys residues.

To determine whether selenium binding results in changes to the protein secondary structure, circular dichroism (CD) spectra were recorded in the far-UV with *At*SBP1 and selenium-bound *At*SBP1 (Fig. 4*B*). The minimum at 217 nm indicates that the secondary structure in the two cases is predominantly β-sheet (49). The binding of selenium has no large impact on the far-UV CD spectra, indicating that the overall secondary structure is not changed by the presence of SeO_3^{2-}. However, small changes can be observed around 230 nm that could be due either to Met or Cys side chains (50, 51), involved in local structures upon ion binding. However, it is not possible to distinguish between these two types of amino acids because they provide very similar negative signals centered on 230 nm (51). These results are well correlated with DTNB analysis suggesting that two Cys residues are involved in selenium binding.

Mass Analysis of AtSBP1 Alone and Purified Selenium-AtSBP1 Complex by Nano-electrospray MS Analysis—To help identify the Cys residues involved in selenium binding, the selenium-*At*SBP1 complex was investigated by mass spectrometry. Direct analysis of the intact (*i.e.* undigested) protein was performed after incubation with and without SeO_3^{2-}, and charge-state profiles were compared. The average mass calculated after deconvolution for *At*SBP1 or selenium-*At*SBP1 is presented in Fig. 5. The calculated mass was 54,184 Da for *At*SBP1 (Fig. 5*A*), which correlates well with a protein folded with a disulfide bridge (−2 Da; the expected mass of the protein is 54,186 Da without a disulfide bridge). These results are supported by the DTNB analysis. In the case of selenium-*At*SBP1 mass analysis, two major species were observed after deconvolution (Fig. 5*B*). The first peak (the minor one), with a mass of 54,185 Da, corresponds to a portion of residual protein with no bound selenium, whereas the second peak (the major one) corresponds to the selenium-bound protein with a mass of 54,262 Da. The difference in mass between *At*SBP1 and selenium-bound *At*SBP1 was 77 Da. This correlates well with the average mass of selenium (78.9 Da) minus the mass of 2 protons indicating that *At*SBP1 reduced SeO_3^{2-} and lost 2 protons from 2 Cys residues. These results further demonstrated the selenium/*At*SBP1 molar ratio was around 1 as shown by ICP-MS and ITC. Furthermore, these data support the ITC experiments that strongly suggested a covalent binding between selenium and *At*SBP1.

Sequence Alignment of SBP Proteins and Three-dimensional Model Analysis of AtSBP1 to Identify Potential Cys Residues Involved in selenium Binding—An alignment of SBPs from diverse organisms together with the 3 SBPs from *A. thaliana* is shown in Fig. 6. Among the three Cys residues that are 100% conserved (Cys^{97}, Cys^{100}, and Cys^{158}; numbering as per *At*SBP1), Cys^{97} and Cys^{100} belong to a C*XX*C motif putatively involved in metal and cadmium binding (37, 52–54). Cys^{484} is highly conserved and only absent in *S. tokodaii* and Cys^{168} is conserved in all photosynthetic organisms (Fig. 5). Two additional Cys residues (Cys^{21} and Cys^{22}) are conserved in all the photosynthetic organisms, and they aligned with a C*XX*C motif in mammals. We also investigated the three-dimensional structure of *At*SBP1 to check whether two Cys residues not adjacent in the sequence could come into contact due to protein folding. The three-dimensional model of *At*SBP1 was modeled using the three-dimensional structure of SBP from *S. tokodaii* (PDB entry 2ECE) (Fig. 7). The model contains residues from Tyr^{29} to Asp^{487}, however, the first 28 residues could not be modeled as they are predicted to be disordered and are not present in the crystal structure. The CD analysis showed that *At*SBP1 secondary structure was predominantly β-sheet, which correlates well with the predicted overall fold of *At*SBP1 that is a β-propeller containing 7 β-sheets, each one composed of four antiparallel β-strands (Fig. 7). DTNB (Fig. 4*A*) and nano-electrospray MS analysis (Fig. 5) indicated the presence of a disulfide bridge that the model predicted between Cys^{97} and Cys^{158} (Fig. 7). DTNB analysis also suggested that four cysteine residues would be reduced and accessible. Based on the model, Cys^{168} would be buried, whereas Cys^{21}, Cys^{22}, Cys^{100}, and Cys^{484} were good candidates to be reduced by DTNB in our experiment. We therefore predicted that in addition to Cys^{21} and Cys^{22}, Cys^{100} and Cys^{484} could be involved in selenium binding.

Identification of AtSBP1 Amino Acids Involved in Selenium Binding by Nano-LC-MS/MS Analysis—To identify the peptide and residues involved in selenium binding in *At*SBP1, fractions containing selenium-bound *At*SBP1 and *At*SBP1 alone were analyzed by nano-LC-MS/MS after a chymotryptic digestion made in solution. The chymotryptic peptide "TMATETEVVAPVTVSNGGSKGCCKY" that contains the two adjacent Cys residues (Cys^{21} and Cys^{22}) was clearly identified as carrying a potential (+selenium, −2H) modification (3 spectra with Mascot score of 33, 39, and 60 identify this modified peptide) (Fig. 8, supplemental Table S1). The same analysis was conducted on a mutated form of the protein where Cys^{21} and Cys^{22} were replaced by serine (supplemental Table S1). The mutated form of the peptide "TMATETEVVAPVTVSNGGSKGSSKY" did not show any binding with selenium. The involvement of Cys^{21} and Cys^{22} in selenium binding was further confirmed by direct measurements of selenium by ICP-MS, on the wild type and mutated version of the protein after incubation with selenium and protein purification. Altogether, these data indicate that selenium binding to *At*SBP1 involved Cys^{21} and Cys^{22}.

Identification of the Local Selenium Environment in AtSBP1 by XANES Analysis—The oxidation state and local environment of selenium in *At*SBP1 was further investigated by x-ray absorption spectroscopy. Fig. 9 compares the selenium K-edge XANES spectra for the selenium-*At*SBP1 complex and for sele-

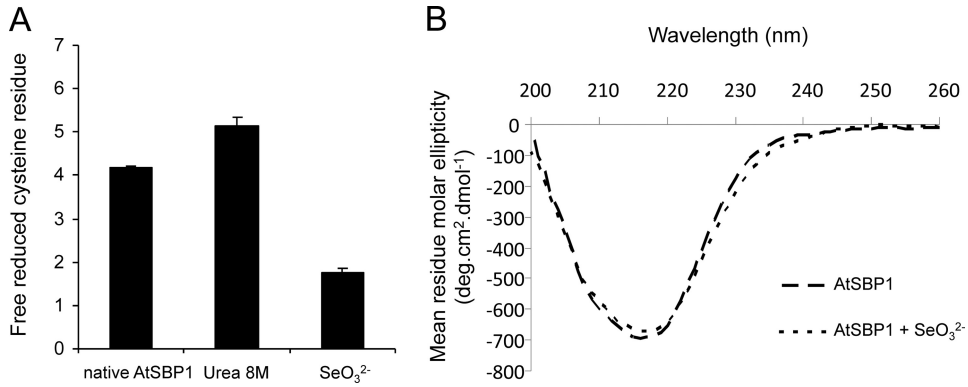

FIGURE 4. **Incubation of *A. thaliana* SBP1 with SeO_3^{2-} indicated modification around cysteine residues.** *A*, quantification of free cysteine residues in *At*SBP1 was performed using Ellmann's reagent (DTNB) in the native condition, in the denaturation condition in the presence of urea, and after a 15-min incubation with SeO_3^{2-}. Data show the mean ± S.D. of 6 independent measurements. *B*, far UV (200–260 nm) circular dichroism recorded from *At*SBP1 and *At*SBP1 incubated with SeO_3^{2-}. Both experiments were performed with a 12.5 ligand/*At*SBP1 molar ratio.

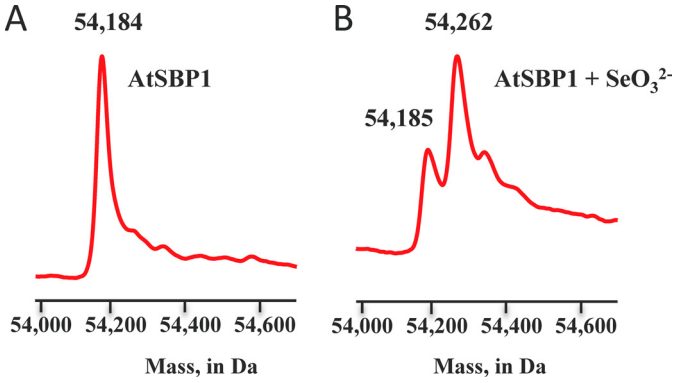

FIGURE 5. **Identification of a 77-Da adduct by comparative direct MS analysis of *A. thaliana* SBP1 before and after a selenium binding assay.** *A* and *B* show the deconvoluted spectra of *At*SBP1 (A) and *At*SBP1 after incubation with SeO_3^{2-} (*B*). For *B*, selenium-bound *At*SBP1 was separated from the free SeO_3^{2-} by steric exclusion chromatography on a Sephadex G-25 column before direct MS analysis. In these experiments, selenium/*At*SBP1 binding ratios were around 0.8 that correlates with the detection of a slight portion of selenium-free *At*SBP1. Mass were calculated from charge states 50 to 40.

nium reference compounds, including SeO_3^{2-}, some organic forms of selenium, SeS_2, and elemental Se(0). The shift in energy of the main peak for Se-*At*SBP1 as compared with SeO_3^{2-} clearly indicates a reduction of SeO_3^{2-} by the protein. The spectrum for the protein was very well reproduced by a one component fit, using 100% selenodiglutathione (R-S-Se(II)-S-R, *R* factor = 0.042, Fig. 9). Adding a second component slightly improved the fit quality (*R* factor = 0.032 to 0.040, with R-Se(II)-R as a second species), but the proportion of this second species was within the precision limit of the method (4 to 8%). These results demonstrate that SeO_3^{2-} in the presence of *At*SBP1 was reduced from the +4 oxidation state to the +2 oxidation state and incorporated in the protein in an R-S-Se(II)-S-R-like conformation. This result is consistent with the involvement of Cys^{21} and Cys^{22} in selenium binding as detailed above.

DISCUSSION

The function of SBPs among different species is not yet clearly established, although their involvement in cancer prevention in humans (20–23, 25–27) and in stress response and detoxification mechanisms in humans and plants (15–17, 35, 38, 55) is well recognized. The proteins are highly conserved between species and present many highly conserved motifs implicated in metal and selenium binding. Our data highlight the chelating properties of *At*SBP1 toward selenium. In addition, we demonstrate the ability of *At*SBP1 to chelate various divalent metal ions. This capacity to bind different ionic species may be linked to a protein function in detoxification mechanisms and in essential metal homeostasis. As a first step to investigate such potential mechanisms, the identification of the ion binding site is necessary. This work led to the identification, for the first time, of the selenium-binding site in SBP1 protein homologues, the description of the oxidation state of bound selenium, and the nature of the amino acids involved. In addition, the work highlights additional potential metal binding sites within the protein.

AtSBP1 Reduces SeO_3^{2-} to Produce a R-S-Se(II)-S-R Bond via Cys^{21} and Cys^{22}—This work shows that the *A. thaliana* homologue to human SBP1 is able to bind selenium *in vitro* when provided as selenite (SeO_3^{2-}) as described for human SBP1 (53). This ability differs from the selenium binding activity of another types of selenium-binding proteins in mammals, not homologous to SBP1, that can bind selenium only when incubated with reduced GSH and SeO_3^{2-}, with binding dependent on the formation of selenodiglutathione prior to interaction with the protein (43, 44, 54). These other types of selenium-binding proteins are involved in the selenium delivery system in mammals, producing the active donor of selenium, "selenophosphate," necessary for the insertion of selenium into selenocysteine and seleno-tRNA required for the formation of selenoproteins.

This work uses a combination of biochemical and biophysical techniques that successfully led to the identification of the selenium-binding site in *At*SBP1. First, ICP-MS performed on the purified selenium-*At*SBP1 complex suggested that the ion to protein molar ratio was 1. This was validated by ITC and nano-electrospray MS analysis that showed that the mass of the complex selenium-*At*SBP1 had gained (+77 Da) compared with *At*SBP1 alone. This was explained by the gain of 1 selenium (+79) and the loss of 2 protons (−2) from two Cys residues. Nano-LC-MS/MS after a chymotryptic digestion of the com-

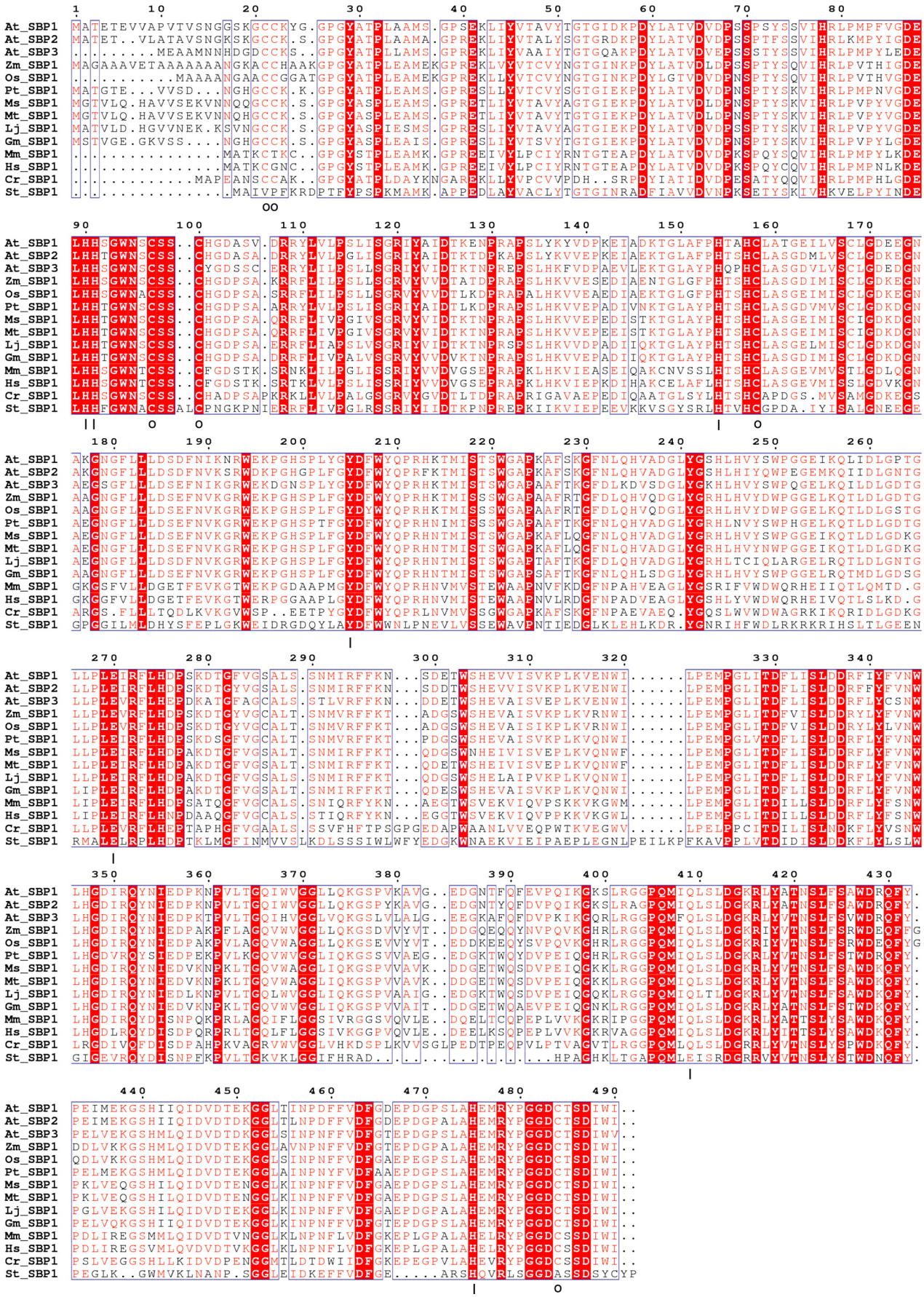
At_SBP1
At_SBP2
At_SBP3
Zm_SBP1
Os_SBP1
Pt_SBP1
Ms_SBP1
Mt_SBP1
Lj_SBP1
Gm_SBP1
Mm_SBP1
Hs_SBP1
Cr_SBP1
St_SBP1

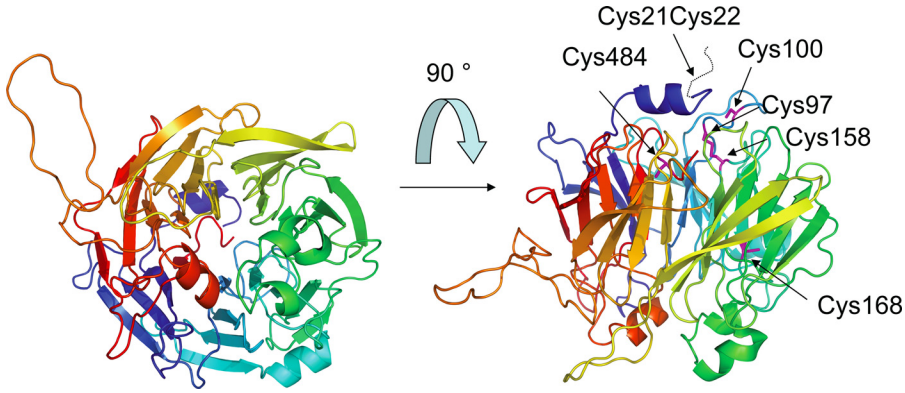

FIGURE 7. **Model of *A. thaliana* SBP1 based on the structure of *S. tokodaii* (PDB entry 2ECE).** The β-strands are represented by *arrows* and the α-helices by *ribbons*. The β-sheets of the β-propeller are colored uniquely. The view of *At*SBP1 after a rotation of 90° highlights the 7 Cys residues. The N and C termini of *At*SBP1 appeared in *blue* and *red*, respectively. Cys residues predicted to be involved in a disulfide bridge (Cys^{97} and Cys^{158}), or buried (Cys^{168}) or accessible (Cys^{100} and Cys^{484}) are labeled. Cys^{21} and Cys^{22}, predicted to be accessible, belong to the N terminus of the protein (from amino acid 1 to 28) represented in *dashed lines* and predicted as disordered.

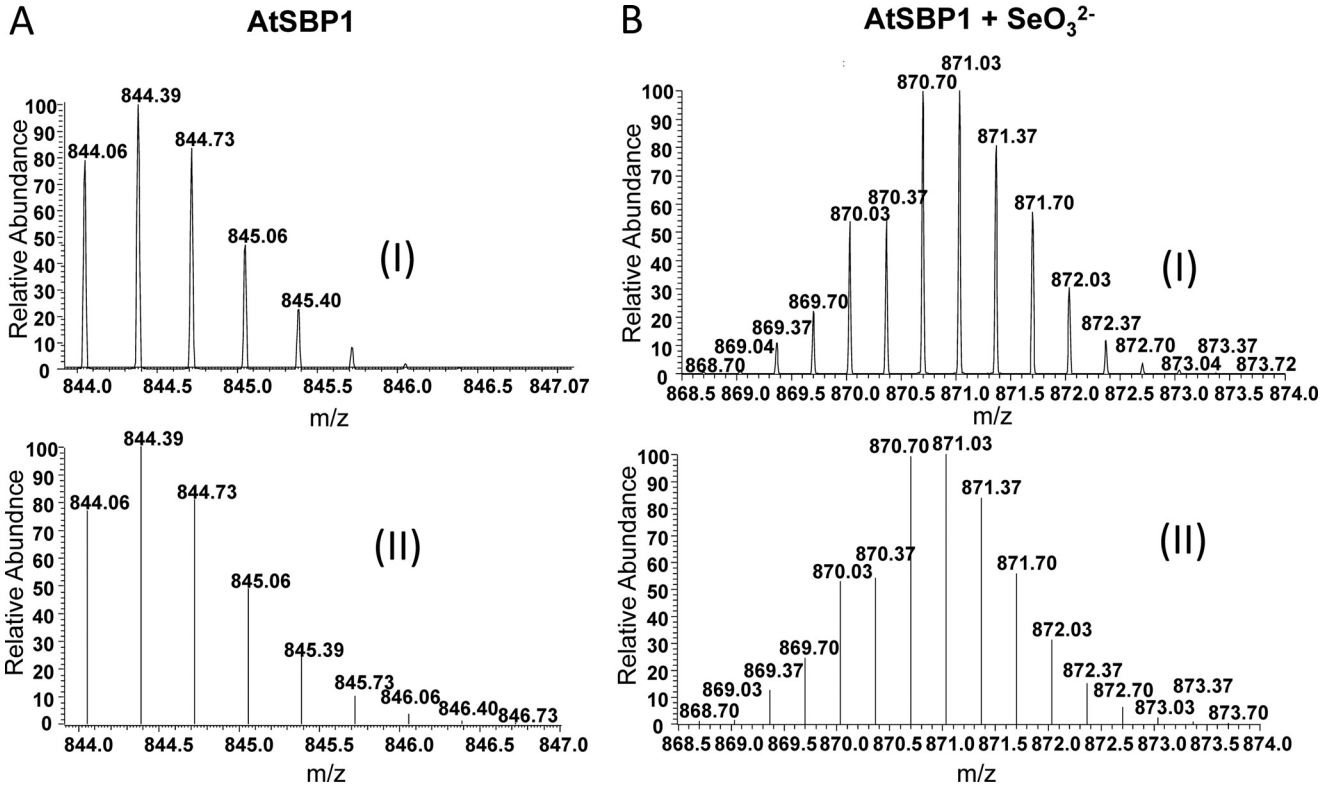

FIGURE 8. **Identification of a selenium adduct on the TMATETEVVAPVTVSNGGSKGCCKY GST-*At*SBP1 chymotrypsic peptide after a selenium binding assay.** *A* and *B* represent T1-Y25 peptide *m/z* spectra isotopic profiles after chymotrypsic digestion of GST-*At*SBP1 (*A*) and selenium-bound GST-*At*SBP1 (*B*) for $z = 3$, (*I*) being the experimental profiles and (*II*) being the theoretical profiles of T1-Y25 peptides. For *B*, selenium-bound protein was separated from the free SeO_3^{2-} by steric exclusion chromatography, on a Sephadex G-25 column before enzyme digestion and nano-LC-MS/MS analysis. We checked that the selenium/GST-*At*SBP1 molar ratio was 1 and that GST alone was not able to bind selenium by ICP-MS and ITC. In the presence of selenium, the obtained masses are in accordance with the theoretical profile of the T1-Y25 chymotryptic peptide with an adduct of +77 (+selenium −2H) at the two vicinal Cys. With no incubation with SeO_3^{2-}, the peptide is oxidized in the level of the two Cys (the formation of this disulfide bridge is explained by the oxidizing conditions during the digestion also triggering observed Met oxidation and deamination of lysine residues).

plex allowed the identification of a unique peptide carrying a (+selenium; −2H) modification. Interestingly, this peptide contained the two adjacent cysteine residues (Cys^{21} and Cys^{22} in *At*SBP1) predicted as good candidates for selenium binding. Cys^{21} and Cys^{22} involvement in SBP1 selenium binding was validated by site-directed mutagenesis. The slight shift in T_m

FIGURE 6. **Sequences alignment of SBP proteins from various organisms.** Alignment was performed using the ClustalW method. Amino acid residues highlighted in *red background* are identical and *blue boxes* delineate highly conserved regions. Symbols and accession numbers are as follows: *At_SBP1–3*, *A. thaliana* (TAIR: At4g14030, At4g14040 and At3g23800); *Zm_SBP1*, *Zea Mays* (NP 001131338); *Os_SBP1*, *Oryza sativa* (Os01g0916400); *Pt_SBP1*, *Populus trichocarpa* (DS 017279); *Ms_SBP1*, *Medicago sativa* (CAC 67501); *Mt_SBP1*, *Medicago truncatula* (CM 001219); *Lj_SBP1*, *L. japonicus* (CAC 67492); *Gm_SBP1*, *Glycine max* (CAC 67472); *Mm_SBP1*, *Mus musculus* (NP 033176); *Hs_SBP1*, *Homo sapiens* (NP 003935); *Cr_SBP1*, *Chlamydomonas reinhardtii* (XP 001703358); *St_SBP1*, *S. tokodaii* (BAB 65016). *Empty circles* indicate Cys residues highly conserved. *Straight lines* indicate the 7 amino acids highly conserved that delineate a central hydrophilic core in *At*SBP1 three-dimensional model.

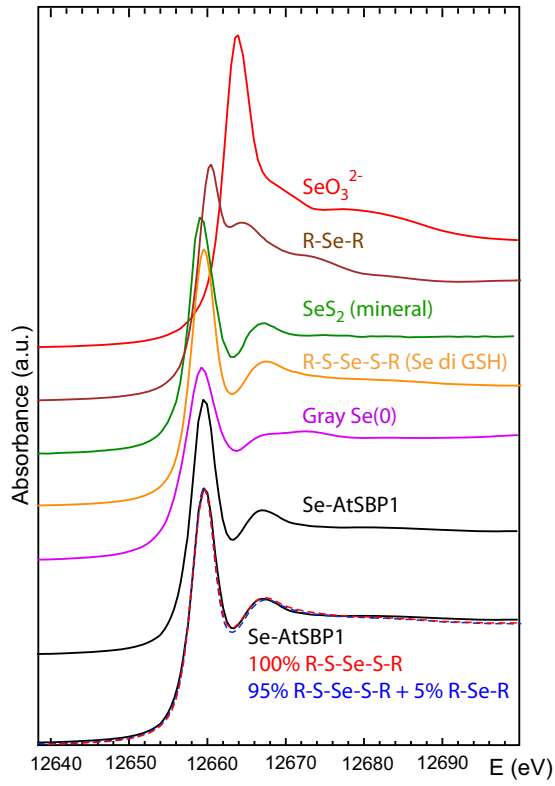

FIGURE 9. **Normalized selenium K-edge XANES spectra for selenium reference compounds, for *A. thaliana* SBP1 incubated in the presence of SeO_3^{2-} and linear combination fits using one (*red*) and two (*blue*) components (*dashed lines*).** Selenium-*At*SBP1 complex was purified by gel filtration before analysis and the ratio selenium/SBP1 of 1 was checked by ICP-MS. From top to bottom: SeO_3^{2-}, selenomethylcysteine- (R-Se-R), selenium disulfide (SeS_2), selenodiglutathione (R-S-Se(II)-S-R), gray elemental selenium (*gray Se(0)*) and selenium-bound *At*SBP1 (*Se-AtSBP1*) alone and with linear combination fits.

upon selenium binding and CD analyses correlated with selenium binding to two adjacent Cys residues.

To characterize the oxidation state and coordination environment of the bound selenium, we used selenium K-edge XANES on purified Se-*At*SBP1. These experiments demonstrated that the selenium coordination environment in *At*SBP1 was identical to the selenium coordination environment in selenodiglutathione. Therefore, *At*SBP1 reduces selenium from a (IV) oxidation state to a (II) oxidation state, and the selenium-binding site in *At*SBP1 involves the two adjacent cysteine residues, Cys^{21} and Cys^{22} that form a R-S-Se(II)-S-R-type bonding environment. The binding of selenium (IV) to SBP1 followed by the reduction to selenium (II) explains the highly exothermic binding enthalpy measured in the ITC experiments.

This work provides the first identification of the selenium-binding site in the SBP1 family of proteins and its speciation within the *Arabidopsis* homologue protein. This binding site has not been characterized in the human SBP1 or in any other organism. These data demonstrate that selenium binding involves a covalent reaction via two cysteine residues in the protein. In human and mouse SBP1 sequences, the two adjacent cysteines responsible for selenium binding in *A. thaliana* are absent and instead a Cys^5-X_2-Cys^8 motif is present. Based on a three-dimensional model of human SBP1 using the *S. tokodaii* three-dimensional structure (PDB entry 2ECE) that was missing the disordered N terminus of SBP1 containing the Cys^5-X_2-Cys^8 motif, it was predicted that Cys^{57} was the only candidate that could be involved on selenium binding in human SBP1 (24). However, Cys^{57} is not conserved among SBP homologues, it is not present in the mouse SBP1 homologue where selenium binding was first characterized nor has the involvement of Cys^{57} in selenium binding been validated experimentally. We therefore propose that in mammals, the two Cys residues within the Cys^5-X_2-Cys^8 motif would be more likely candidates for binding selenium that Cys^{57} alone. This hypothesis will be very interesting to test in future work.

Physiological Function of Selenium Binding in AtSBP1—Selenium is not essential to land plants although beneficial effects are reported (see Introduction). However, *At*SBP1 has kept the ability to bind selenium *in vitro*, and *At*SBP1 over-expression enhances tolerance to selenium (15). The selenium binding motif "Cys-Cys" in *At*SBP1 is conserved in all photosynthetic organisms. Most plants and soil contain traces of selenium, and for cereals, as an example, selenium content ranges from 0.1 to 3 μmol/kg of fresh weight (3). We previously showed that *At*SBP1 was expressed early during plant development and constitutively expressed in healthy adult plants (35). A similar pattern of expression was reported in *Lotus japonicus* (16). *At*SBP1 concentration in roots has been estimated to be around 0.09 μmol/kg of fresh weight and can be 5 to 10 times higher in response to inducible stresses. Based on these observations and the molar binding ratio of 1:1 between selenium and *At*SBP1, it is likely that *At*SBP1, by chelating selenium, acts as a selenium detoxifying mechanism, when plants are grown in soil containing trace amounts of selenium. Selenium metabolism in plants is quite well described and understood due to the similarity between selenium and sulfur (7, 11, 13). Up to now, reduction of selenite to selenide in the cytosol is believed to happen nonenzymatically via GSH (7). *At*SBP1, by reducing selenite, would avoid selenite reduction by GSH, therefore preventing selenium from interfering with sulfur metabolism by incorporation in proteins via selenium-Met and selenium-Cys formation. Selenite is highly toxic and any mechanism preventing its accumulation may be very helpful in reducing its toxicity. The ability of *At*SBP1 to reduce selenite is another example of the functional similarity between *At*SBP1 and GSH that was previously observed (see Introduction). An important question, which remains, is what is happening to selenium once bound to *At*SBP1? Is it transferred to a donor or to another cellular compartment, which would allow SBP1 to reduce another selenium and thus increase its ability to detoxify greater concentrations of selenium? These points still need to be investigated to better understand the function of *At*SBP1 in selenium metabolism and detoxification.

Physiological Function of SBP1 in Response to Metallic Stress—This work and previous studies (35) showed that *At*SBP1 was able to bind SeO_3^{2-} and Cd^{2+} that are not essential in land plants. The apparent binding constant for selenium was 1.6 μM based on ITC measurements. Using TSA and ICP-MS, we showed that *At*SBP1 has chelating properties toward different essential metals, such as zinc, copper, and cobalt. Although the affinities of SBP1 for these ligands still need to be investigated, an additional function of SBP1 may therefore be linked to

essential metal homeostasis. When we looked at the alignment of various SBP1 homologues we also noted other highly conserved putative metal binding motifs (58, 59). Among the 17 histidines present in *At*SBP1, His^{78}, His^{90}, His^{91}, His^{154}, His^{157}, and His^{475} are 100% conserved among all the SBP sequences. In the three-dimensional structure of SBP1, the 7 β-sheets delineate a central hydrophilic core containing four conserved His residues (His^{90}, His^{91}, His^{154}, His^{475}), and the highly conserved residues Tyr^{205}, Glu^{270}, and Gln^{409} (data not shown). In the SBP structure from *S. tokodaii*, the corresponding residues (His^{74}, His^{75}, His^{141}, His^{445}, Tyr^{191}, Glu^{255}, and Gln^{384}) are present and bound to water molecules. These seven residues facing the cavity are 100% conserved among all the SBPs. Although the function of β-propeller folded proteins is very large, the central pore is often important for ligand binding and/or catalysis of the protein (60). In *Loligo vulgaris*, for example, the cavity of the diisopropylfluorophosphatase (DFPase) coordinates 2 Ca^{2+}, which are important for the protein function (61, 62). The *At*SBP1 central cavity is therefore very attractive as an additional potential metal-binding site.

Conclusion—SBP1 over-expression in *A. thaliana* enhances tolerance to various stresses including selenium. In the present work, we identify the selenium-binding site in *At*SBP1. These data provide a better understanding of the putative function of *At*SBP1 in selenium metabolism and detoxification. The identification of the amino acids involved in selenium binding will help clarify the link between the observed phenotype of enhanced selenium tolerance in *At*SBP1 over-expressing plants. The involvement of Cys^{21}/Cys^{22} in selenium accumulation in *At*SBP1 is of great interest due to its potential use in phyto remediation processes and biofortification. Mammalian SBP1s bear a similar cysteine-rich motif at their N-terminal regions and this likely denotes the bona fide selenium-binding site.

Acknowledgments—We acknowledge the ESRF for beamtime and technical support. We thank Alexandra Kraut and Christophe Masselon (CEA Grenoble) for their help in mass spectrometry analyses and Sylvie Motelier (CEA Grenoble) for help in ICP-MS analyses.

REFERENCES

1. Behne, D., and Kyriakopoulos, A. (2001) Mammalian selenium-containing proteins. *Annu. Rev. Nutr.* **21,** 453–473
2. Fu, L. H., Wang, X. F., Eyal, Y., She, Y. M., Donald, L. J., Standing, K. G., and Ben-Hayyim, G. (2002) A selenoprotein in the plant kingdom: mass spectrometry confirms that an opal codon (UGA) encodes selenocysteine in *Chlamydomonas reinhardtii* gluththione peroxidase. *J. Biol. Chem.* **277,** 25983–25991
3. Mehdi, Y., Hornick, J. L., Istasse, L., and Dufrasne, I. (2013) Selenium in the environment, metabolism and involvement in body functions. *Molecules* **18,** 3292–3311
4. Papp, L. V., Lu, J., Holmgren, A., and Khanna, K. K. (2007) From selenium to selenoproteins: synthesis, identity, and their role in human health. *Antioxid. Redox. Signal* **9,** 775–806
5. Zhu, Y. G., Pilon-Smits, E. A., Zhao, F. J., Williams, P. N., and Meharg, A. A. (2009) Selenium in higher plants: understanding mechanisms for biofortification and phytoremediation. *Trends Plant Sci.* **14,** 436–442
6. Ellis, D. R., and Salt, D. E. (2003) Plants, selenium and human health. *Curr. Opin. Plant. Biol.* **6,** 273–279
7. Sors, T. G., Ellis, D. R., and Salt, D. E. (2005) Selenium uptake, translocation, assimilation and metabolic fate in plants. *Photosynth Res.* **86,** 373–389
8. Pilon-Smits, E. A., and LeDuc, D. L. (2009) Phytoremediation of selenium using transgenic plants. *Curr. Opin. Biotechnol.* **20,** 207–212
9. Feng, R. W., Wei, C. Y., and Tu, S. X. (2013) The roles of selenium in protecting plants against abiotic stresses. *Environ. Exp. Bot.* **87,** 58–68
10. Pilon-Smits, E. A., Quinn, C. F., Tapken, W., Malagoli, M., and Schiavon, M. (2009) Physiological functions of beneficial elements. *Curr. Opin. Plant Biol.* **12,** 267–274
11. Terry, N., Zayed, A. M., De Souza, M. P., and Tarun, A. S. (2000) Selenium in higher plants. *Annu. Rev. Plant Physiol. Plant Mol. Biol.* **51,** 401–432
12. Van Hoewyk, D. (2013) A tale of two toxicities: malformed selenoproteins and oxidative stress both contribute to selenium stress in plants. *Ann. Bot.* **112,** 965–972
13. White, P. J., Bowen, H. C., Parmaguru, P., Fritz, M., Spracklen, W. P., Spiby, R. E., Meacham, M. C., Mead, A., Harriman, M., Trueman, L. J., Smith, B. M., Thomas, B., and Broadley, M. R. (2004) Interactions between selenium and sulphur nutrition in Arabidopsis thaliana. *J. Exp. Bot.* **55,** 1927–1937
14. Bansal, M. P., Mukhopadhyay, T., Scott, J., Cook, R. G., Mukhopadhyay, R., and Medina, D. (1990) DNA sequencing of a mouse liver protein that binds selenium: implications for selenium's mechanism of action in cancer prevention. *Carcinogenesis* **11,** 2071–2073
15. Agalou, A., Roussis, A., and Spaink, H. P. (2005) The *Arabidopsis* selenium-binding protein confers tolerance to toxic levels of selenium. *Funct. Plant Biol.* **32,** 881–890
16. Flemetakis, E., Agalou, A., Kavroulakis, N., Dimou, M., Martsikovskaya, A., Slater, A., Spaink, H. P., Roussis, A., and Katinakis, P. (2002) Lotus japonicus gene Ljsbp is highly conserved among plants and animals and encodes a homologue to the mammalian selenium-binding proteins. *Mol. Plant Microbe Interact.* **15,** 313–322
17. Sawada, K., Hasegawa, M., Tokuda, L., Kameyama, J., Kodama, O., Kohchi, T., Yoshida, K., and Shinmyo, A. (2004) Enhanced resistance to blast fungus and bacterial blight in transgenic rice constitutively expressing OsSBP, a rice homologue of mammalian selenium-binding proteins. *Biosci. Biotechnol. Biochem.* **68,** 873–880
18. Song, L., Zou, H., Chang, Y., Xu, W., and Wu, L. (2006) The cDNA cloning and mRNA expression of a potential selenium-binding protein gene in the scallop *Chlamys farreri*. *Dev. Comp. Immunol.* **30,** 265–273
19. Ansong, E., Yang, W., and Diamond, A. M. (2014) Molecular cross-talk between members of distinct families of selenium containing proteins. *Mol. Nutr. Food Res.* **58,** 117–123
20. Chen, G., Wang, H., Miller, C. T., Thomas, D. G., Gharib, T. G., Misek, D. E., Giordano, T. J., Orringer, M. B., Hanash, S. M., and Beer, D. G. (2004) Reduced selenium-binding protein I expression is associated with poor outcome in lung adenocarcinomas. *J. Pathol.* **202,** 321–329
21. Huang, C., Ding, G., Gu, C., Zhou, J., Kuang, M., Ji, Y., He, Y., Kondo, T., and Fan, J. (2012) Decreased selenium-binding protein 1 enhances glutathione peroxidase 1 activity and downregulates HIF-1α to promote hepatocellular carcinoma invasiveness. *Clin. Cancer Res.* **18,** 3042–3053
22. Kim, H., Kang, H. J., You, K. T., Kim, S. H., Lee, K. Y., Kim, T. I., Kim, C., Song, S. Y., Kim, H. J., and Lee, C. (2006) Suppression of human selenium-binding protein 1 is a late event in colorectal carcinogenesis and is associated with poor survival. *Proteomics* **6,** 3466–3476
23. Pohl, N. M., Tong, C., Fang, W., Bi, X., Li, T., and Yang, W. (2009) Transcriptional regulation and biological functions of selenium-binding protein 1 in colorectal cancer *in vitro* and in nude mouse xenografts. *Plos One* **4,** e7774
24. Raucci, R., Colonna, G., Guerriero, E., Capone, F., Accardo, M., Castello, G., and Costantini, S. (2011) Structural and functional studies of the human selenium binding protein-1 and its involvement in hepatocellular carcinoma. *Biochim. Biophys. Acta* **1814,** 513–522
25. Silvers, A. L., Lin, L., Bass, A. J., Chen, G., Wang, Z., Thomas, D. G., Lin, J., Giordano, T. J., Orringer, M. B., Beer, D. G., and Chang, A. C. (2010) Decreased selenium-binding protein 1 in esophageal adenocarcinoma results from posttranscriptional and epigenetic regulation and affects chemosensitivity. *Clin. Cancer Res.* **16,** 2009–2021
26. Xia, Y. J., Ma, Y. Y., He, X. J., Wang, H. J., Ye, Z. Y., and Tao, H. Q. (2011)

Suppression of selenium-binding protein 1 in gastric cancer is associated with poor survival. *Hum. Pathol.* **42,** 1620–1628
27. Zhang, S., Li, F., Younes, M., Liu, H., Chen, C., and Yao, Q. (2013) Reduced selenium-binding protein 1 in breast cancer correlates with poor survival and resistance to the anti-proliferative effects of selenium. *Plos One* **8,** e63702
28. Fang, W., Goldberg, M. L., Pohl, N. M., Bi, X., Tong, C., Xiong, B., Koh, T. J., Diamond, A. M., and Yang, W. (2010) Functional and physical interaction between the selenium-binding protein 1 (SBP1) and the glutathione peroxidase 1 selenoprotein. *Carcinogenesis* **31,** 1360–1366
29. Glatt, S. J., Everall, I. P., Kremen, W. S., Corbeil, J., Sásik, R., Khanlou, N., Han, M., Liew, C. C., and Tsuang, M. T. (2005) Comparative gene expression analysis of blood and brain provides concurrent validation of SELENBP1 up-regulation in schizophrenia. *Proc. Natl. Acad. Sci. U.S.A.* **102,** 15533–15538
30. Kanazawa, T., Chana, G., Glatt, S. J., Mizuno, H., Masliah, E., Yoneda, H., Tsuang, M. T., and Everall, I. P. (2008) The utility of *SELENBP1* gene expression as a biomarker for major psychotic disorders: replication in schizophrenia and extension to bipolar disorder with psychosis. *Am. J. Med. Genet. B Neuropsychiatr. Genet.* **147B,** 686–689
31. Porat, A., Sagiv, Y., and Elazar, Z. (2000) A 56-kDa selenium-binding protein participates in intra-Golgi protein transport. *J. Biol. Chem.* **275,** 14457–14465
32. Cohen, S. D., Pumford, N. R., Khairallah, E. A., Boekelheide, K., Pohl, L. R., Amouzadeh, H. R., and Hinson, J. A. (1997) Selective protein covalent binding and target organ toxicity. *Toxicol. Appl. Pharmacol.* **143,** 1–12
33. Lanfear, J., Fleming, J., Walker, M., and Harrison, P. (1993) Different patterns of regulation of the genes encoding the closely related 56-kDa selenium-binding and acetaminophen-binding proteins in normal-tissues and during carcinogenesis. *Carcinogenesis* **14,** 335–340
34. Mattow, J., Demuth, I., Haeselbarth, G., Jungblut, P. R., and Klose, J. (2006) Selenium-binding protein 2, the major hepatic target for acetaminophen, shows sex differences in protein abundance. *Electrophoresis* **27,** 1683–1691
35. Dutilleul, C., Jourdain, A., Bourguignon, J., and Hugouvieux, V. (2008) The *Arabidopsis* putative selenium-binding protein family: expression study and characterization of SBP1 as a potential new player in cadmium detoxification processes. *Plant Physiol.* **147,** 239–251
36. Sarry, J. E., Kuhn, L., Ducruix, C., Lafaye, A., Junot, C., Hugouvieux, V., Jourdain, A., Bastien, O., Fievet, J. B., Vailhen, D., Amekraz, B., Moulin, C., Ezan, E., Garin, J., and Bourguignon, J. (2006) The early responses of *Arabidopsis thaliana* cells to cadmium exposure explored by protein and metabolite profiling analyses. *Proteomics* **6,** 2180–2198
37. Pal, R., and Rai, J. P. (2010) Phytochelatins: peptides involved in heavy metal detoxification. *Appl. Biochem. Biotechnol.* **160,** 945–963
38. Hugouvieux, V., Dutilleul, C., Jourdain, A., Reynaud, F., Lopez, V., and Bourguignon, J. (2009) *Arabidopsis* putative selenium-binding protein1 expression is tightly linked to cellular sulfur demand and can reduce sensitivity to stresses requiring glutathione for tolerance. *Plant Physiol.* **151,** 768–781
39. Noctor, G., Mhamdi, A., Chaouch, S., Han, Y., Neukermans, J., Marquez-Garcia, B., Queval, G., and Foyer, C. H. (2012) Glutathione in plants: an integrated overview. *Plant Cell Environ.* **35,** 454–484
40. Niesen, F. H., Berglund, H., and Vedadi, M. (2007) The use of differential scanning fluorimetry to detect ligand interactions that promote protein stability. *Nat. Protoc.* **2,** 2212–2221
41. Dupierris, V., Masselon, C., Court, M., Kieffer-Jaquinod, S., and Bruley, C. (2009) A toolbox for validation of mass spectrometry peptides identification and generation of database: IRMa. *Bioinformatics* **25,** 1980–1981
42. Proux, O., Biquard, X., Lahera, E., Menthonnex, J. J., Prat, A., Ulrich, O., Soldo, Y., Trevisson, P., Kapoujyan, G., Perroux, G., Taunier, P., Grand, D., Jeantet, P., Deleglise, M., Roux, J. P., and Hazemann, J. L. (2005) FAME: a new beamline for X-ray absorption investigations of very-diluted systems of environmental, material and biological interests. *Phys. Scripta* **115,** 970–973
43. Sarret, G., Avoscan, L., Carrière, M., Collins, R., Geoffroy, N., Carrot, F., Covès, J., and Gouget, B. (2005) Chemical forms of selenium in the metal-resistant bacterium *Ralstonia metallidurans* CH34 exposed to selenite and selenate. *Appl. Environ. Microbiol.* **71,** 2331–2337
44. Brazier, M. W., Davies, P., Player, E., Marken, F., Viles, J. H., and Brown, D. R. (2008) Manganese binding to the prion protein. *J. Biol. Chem.* **283,** 12831–12839
45. Lai, B., Li, Y., Cao, A., and Lai, L. (2003) Metal ion binding and enzymatic mechanism of *Methanococcus jannaschii* RNase HII. *Biochemistry* **42,** 785–791
46. Crépin, T., Dias, A., Palencia, A., Swale, C., Cusack, S., and Ruigrok, R. W. (2010) Mutational and metal binding analysis of the endonuclease domain of the influenza virus polymerase PA subunit. *J. Virol.* **84,** 9096–9104
47. Ogasawara, Y., Lacourciere, G., and Stadtman, T. C. (2001) Formation of a selenium-substituted rhodanese by reaction with selenite and glutathione: possible role of a protein perselenide in a selenium delivery system. *Proc. Natl. Acad. Sci. U.S.A.* **98,** 9494–9498
48. Ogasawara, Y., Lacourciere, G. M., Ishii, K., and Stadtman, T. C. (2005) Characterization of potential selenium-binding proteins in the selenophosphate synthetase system. *Proc. Natl. Acad. Sci. U.S.A.* **102,** 1012–1016
49. Kelly, S. M., Jess, T. J., and Price, N. C. (2005) How to study proteins by circular dichroism. *Biochim. Biophys. Acta* **1751,** 119–139
50. Chaffotte, A. F., Guillou, Y., and Goldberg, M. E. (1992) Kinetic resolution of peptide bond and side chain far-UV circular dichroism during the folding of hen egg white lysozyme. *Biochemistry* **31,** 9694–9702
51. Krittanai, C., and Johnson, W. C. (1997) Correcting the circular dichroism spectra of peptides for contributions of absorbing side chains. *Anal. Biochem.* **253,** 57–64
52. Suzuki, N., Yamaguchi, Y., Koizumi, N., and Sano, H. (2002) Functional characterization of a heavy metal binding protein CdI19 from *Arabidopsis*. *Plant J.* **32,** 165–173
53. Dian, C., Vitale, S., Leonard, G. A., Bahlawane, C., Fauquant, C., Leduc, D., Muller, C., de Reuse, H., Michaud-Soret, I., and Terradot, L. (2011) The structure of the *Helicobacter pylori* ferric uptake regulator Fur reveals three functional metal binding sites. *Mol. Microbiol.* **79,** 1260–1275
54. Sutherland, D. E., and Stillman, M. J. (2011) The "magic numbers" of metallothionein. *Metallomics* **3,** 444–463
55. Agalou, A., Spaink, H. P., and Roussis, A. (2006) Novel interaction of selenium-binding protein with glyceraldehyde-3-phosphate dehydrogenase and fructose-bisphosphate aldolase of *Arabidopsis thaliana*. *Funct. Plant Biol.* **33,** 847–856
56. Jeong, J. Y., Wang, Y., and Sytkowski, A. J. (2009) Human selenium binding protein-1 (hSP56) interacts with VDU1 in a selenium-dependent manner. *Biochem. Biophys. Res. Commun.* **379,** 583–588
57. Suzuki, M., Lee, D. Y., Inyamah, N., Stadtman, T. C., and Tjandra, N. (2008) Solution NMR structure of selenium-binding protein from *Methanococcus vannielii*. *J. Biol. Chem.* **283,** 25936–25943
58. Tainer, J. A., Roberts, V. A., and Getzoff, E. D. (1991) Metal-binding sites in proteins. *Curr. Opin. Biotechnol.* **2,** 582–591
59. Tainer, J. A., Roberts, V. A., and Getzoff, E. D. (1992) Protein metal-binding sites. *Curr. Opin. Biotechnol.* **3,** 378–387
60. Pons, T., Gómez, R., Chinea, G., and Valencia, A. (2003) β-Propellers: associated functions and their role in human diseases. *Curr. Med. Chem.* **10,** 505–524
61. Hartleib, J., Geschwindner, S., Scharff, E. I., and Rüterjans, H. (2001) Role of calcium ions in the structure and function of the di-isopropylfluorophosphatase from Loligo vulgaris. *Biochem. J.* **353,** 579–589
62. Scharff, E. I., Koepke, J., Fritzsch, G., Lücke, C., and Rüterjans, H. (2001) Crystal structure of diisopropylfluorophosphatase from *Loligo vulgaris*. *Structure* **9,** 493–502